Evidence from infrared dichroism, x-ray diffraction, and atomistic computer simulation for a ''zigzag'' molecular shape in tilted smectic liquid crystal phases

W. G. Jang, M. A. Glaser, C. S. Park, K. H. Kim, Y. Lansac, and N. A. Clark

Ferroelectric Liquid Crystal Materials Research Center, Department of Physics, University of Colorado, Boulder, Colorado 80309-0390

Infrared dichroism (IR) and atomistic computer simulation are employed to probe molecular shape in smectic liquid crystal phases where the optic axis is tilted relative to the layer normal. Polar plots of absorption profiles due to core (phenyl, C-C) and tail (alkyl or methylene, CH_2) vibrations in the tilted synclinic (smectic-C) phase of a variety of materials show the phenyl (core) IR absorbance symmetry axes to be consistently tilted at larger angle from the layer normal than the alkyl or methylene (tail). This suggests that, on average, the tails are less tilted than the cores. Furthermore, we find that optic axis tilt angle is close to the core tilt angle measured by IR dichroism, as expected, since liquid crystal birefringence arises primarily from the cores. These results are in accord with the ''zigzag'' model of Bartolino, Doucet, and Durand. However, we find that only a small fraction of the tail, the part nearest the core, is tilted, and only this part contributes significantly to layer contraction upon molecular tilt.

I. INTRODUCTION

The basic tilted smectic liquid crystal phase, the smectic-C (Sm-C), is characterized by the structure shown in Fig. 1, a one-dimensional (1D) stacking of 2D liquid layers of rod-shaped molecules having a mean long molecular axis (optic axis) tilted through a fixed angle θ from the layer normal and having synclinic orientation of the tilt in adjacent planes. If such a phase is made from chiral molecules, then the lack of mirror symmetry requires it to have a macroscopic spontaneous polarization $\mathbf{P}_s$, locally normal to the mean long axis $\mathbf{n}$ and to the layer normal $\mathbf{z}$ [1]. Although the magnitude of $\mathbf{P}_s$ is fixed, depending only on temperature, the azimuthal orientation $\phi(\mathbf{r})$ responds to applied electric field, surface interactions, and elasticity of the director field $\mathbf{n}(\mathbf{r})$. The demonstration of fast, bistable electro-optic effects based on the electric-field coupling to $\mathbf{P}_s$ to control $\phi(\mathbf{r})$ in the bookshelf surface-stabilized ferroelectric liquid crystal cell geometry of Fig. 1 [2] has led to intense interest in understanding the molecular organization in such phases, a requirement for the directed design of useful materials.

The experimental study of molecular shape in tilted smectic was begun by Bartolino, Doucet, and Durand (BDD), who noted that the layer shrinkage from molecular tilt accompanying the Sm-C phase, observable in x-ray diffraction, is smaller than that calculated on the basis of the optic axis tilt [3]. They proposed a ''zigzag'' molecular shape, with the tails less tilted than the cores to account for this observation, which has since been confirmed in other materials [4]. This zigzag proposal has been employed as an element in the ''Boulder model,'' a tool for the design of chiral ferroelectric smectic materials. In the Boulder model, molecules are confined, either orientationally or positionally by a mean field (binding site) generated by their neighbors in the phase. Following BDD, the binding site takes a bent (zigzag) cylinder shape in which tails are less tilted than the cores. According to the Boulder model [5–8], given the Sm-C two-fold axes, parallel to $\mathbf{x}$ in the layer midplanes, the mean molecular or-

ganization with tails less tilted than cores implies that the molecular mean field or binding site imposed on a molecule by its neighbors is zigzag shaped (zigzag bent cylindrical hole), and leads to a natural explanation of the polar ordering about the molecular long axis in the Sm-C phase, since, in general, only a single orientation of a bent molecular conformation about its long axis will minimize energy in a zigzag shaped binding site. Confinement of any calamitic molecule in such a binding site thus results in polar orientational order about the long molecular axis. That is, at least some interatomic bond vectors will have nonzero average components in the layer plane [5,9]. If the molecule is chiral, then this polar ordering produces a net molecular dipole in the layer
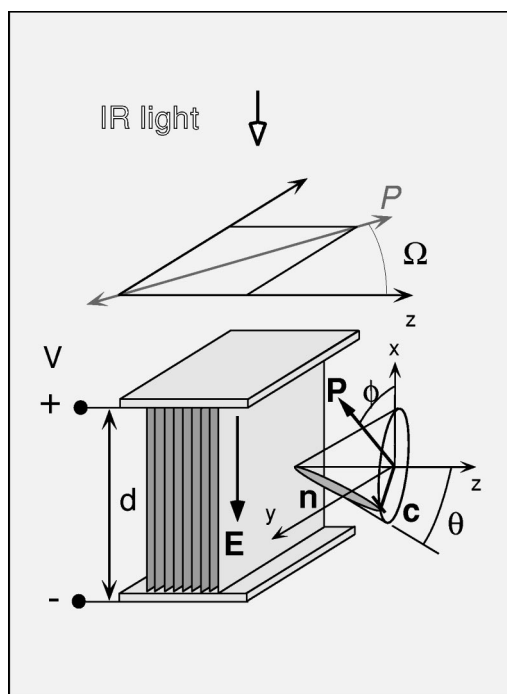
FIG. 1. Chemical structures and phase diagrams of the ferroelectric liquid crystal materials used in this experiments.

(a)

(b)
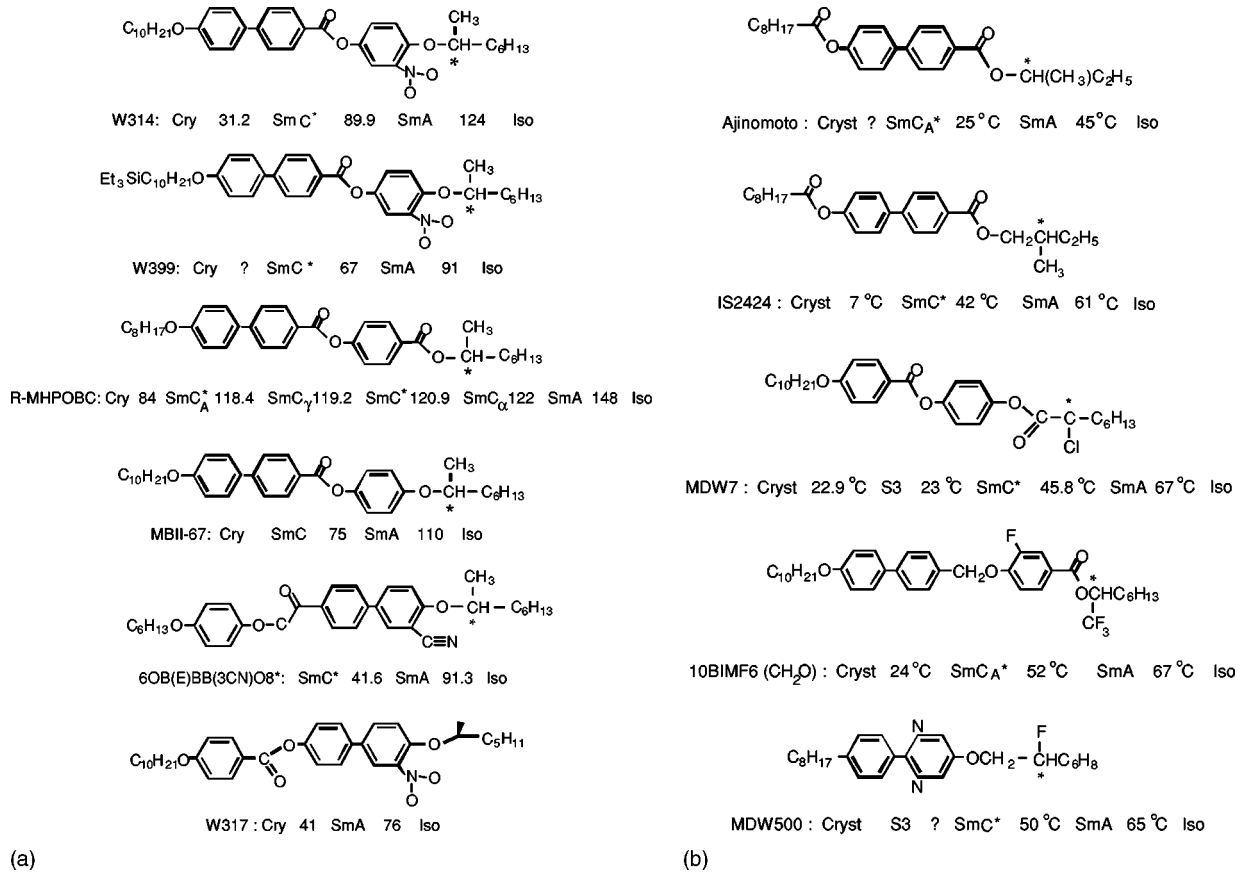
FIG. 2. A schematic diagram of the FTIR experimental setup.

plane and normal to the tilt plane. Thus, the ferroelectric polarization is determined by the equilibrium distribution of bent conformers in an ensemble of zigzag binding sites. This kind of mean-field picture leads to a technique for prediction of the ferroelectric polarization, using atomistic simulation to equilibrate single molecules in zigzag mean-field potentials [10,11]. The quantitative agreement of polarization sign and magnitude calculated with a binding site having the tails less tilted than the cores with measured values is evidence that the tails are less tilted than the cores in tilted smectics. Atomistic molecular-dynamics and Monte Carlo simulation of bulk smectic phases also indicates that the typical alkyl tails are less tilted than cores. Here, we demonstrate that infrared (IR) dichroism may directly probe the relative mean tilt of cores and tails in a tilted smectic phase.

Recently, infrared (IR) dichroism has proven to be a powerful probe of the molecular conformation and organization in liquid crystal phases [12–15]. IR spectroscopy selects molecular vibrational modes via the coupling of IR light to mode transition dipoles, which are fixed on the molecule or a molecular subfragment. Measurement of IR absorbance vs polarization orientation relative to the symmetry axes of a macroscopically single domain sample then enables the moments of the transition dipole, and, therefore, of the molecular orientation distribution to be determined. It is particularly interesting to apply this technique to the lower-symmetry LC phases, such as the smectic-C (Sm-C), in which there is polar ordering of molecular subfragments, and the ferroelec-

tric liquid crystal (FLC) chiral smectic-C (Sm-C), which is macroscopically polar. Recently, Fourier transform infrared (FTIR) studies of FLC's have probed the origin of ferroelectricity via static dichroism measurements [12–14].

II. EXPERIMENTS

The liquid crystal materials studied in this paper represent a diverse collection with the common feature of having tilted chiral smectic phases, and specifically, the smectic-C phase, either as a ground state, or induced by field. They are W314 [16,17], W399 [18], W317 [14,19], MHPOBC [20,32], IS2424 [21,22], MDW7 [23], MDW500 [23], MBII-67 [24], Ajinomoto [25], 10BIMF6(CH_2O) [26], and 6OB(E)BB(3CN)O8* [27] as shown in Fig. 2. W314 and W399 show the smectic-C phase at room temperature and have the electro-negative polar substituent -NO_2 on a core ring near the chiral tail to provide a high-negative ferroelectric polarization $|\mathbf{P}_s|$ as large as 426 nC/cm^2 and fast switching [17]. MBII-67 is the W314 homolog without the -NO_2. W317 exhibits large electroclinic effects and dynamic FTIR experiments have been carried out on it [14]. MHPOBC exhibits an antiferroelectric Sm-C_A phase and ferrielectric Sm-C_α and Sm-C_γ phases, and was the first reported Sm-C_A material [20]. Compounds IS2424 and MDW500 show polarization inversion at temperatures in smectic-C phase. The Ajinomoto material shows monotropic phase, 10BIMF6(CH_2O) exhibits antiferroelectric phases, and

6OB(E)BB(3CN)O8 has a cyano (C≡N) group on the phenyl ring that is believed to give its large polarization.

The experimental cell geometry, represented in Fig. 1, has the LC as the dielectric in an IR transparent capacitor, and planar (bookshelf) alignment of the layers. This cell geometry, with the IR light incident along **x**, normal to the cell [14], is very useful for probing the response of molecular orientation to applied, field via IR dichroism. With field applied the Sm-*C* tilt plane (defined as being parallel to **n** and **z**) is normal to the incident IR light propagation direction, so that by varying the IR polarization, the orientation of the projection of the absorption dipoles onto the tilt plane may be probed.

A wire-grid IR polarizer is positioned between IR source and sample and its orientation Ω, is set at under computer control, with $\Omega=0°$ having IR polarization parallel to layer normal. The electro-optic cells were IR and visible-light transparent, made from CaF_2 windows coated with a thin layer of indium-tin oxide (ITO) for electrodes and spaced to a LC thickness of $2<d<3$ μm by uniform polymer balls. The ITO was spin coated with a 200 Å, thick nylon film that was buffed to align the LC. The cells were filled with LC's in the isotropic phase and cooled slowly into the Sm-*A* and Sm-*C* phases. Alignment quality was checked with visible-light polarized microscopy. The layer structure obtained upon cooling into the Sm-*C* phase was chevron, but the voltage threshold for deforming the chevron structure into the bookshelf was generally quite low in these high-polarization materials (several volts), so that the IR experiments were always carried out in the bookshelf geometry, i.e., with the smectic layers normal to the plates. In the Sm-*C* phase, IR dichroism and visible-light birefringence were measured with a square-wave voltage of sufficiently large amplitude applied to the cell geometry of Fig. 1, such that $\mathbf{n}(\mathbf{r})$ is spatially uniform, driven by the field around on the tilt cone to saturation at $\phi=0$ for $\phi=\pi$. The visible-light optic axis tilt angle θ was taken to be the polarizer orientation relative to **z** for extinction, with the cell between crossed polarizer analyzer.

X-ray scattering was carried out on beamline X10A at NSLS (National Synchrotron Light Source) at Brookhaven National Laboratory. Powder (unoriented) samples were contained in 1 mm diameter capillaries and placed in a temperature-controlled oven on a diffractometer with a Si (111) monochrometer and Ge (111) analyzer. Wave-vector resolution was 0.0004 Å.

III. RESULTS AND DISCUSSION

A. Infrared Dichroism

It is not possible to extract molecular orientation parameters from data taken at a single polarizer orientation Ω. Hence, for full data collection, peak absorbance for each vibration is obtained by fits to the spectra for a series of Ω, spaced by 10° intervals. Typical results, in this case for W314 at T=100 °C in the smectic-*A* (Sm-*A*) phase and at T=70 °C in the Sm-*C* phase, are displayed in Fig. 3 as polar plots of peak absorbance $A(\Omega)$ vs Ω for the *alkyl* tail CH$_2$
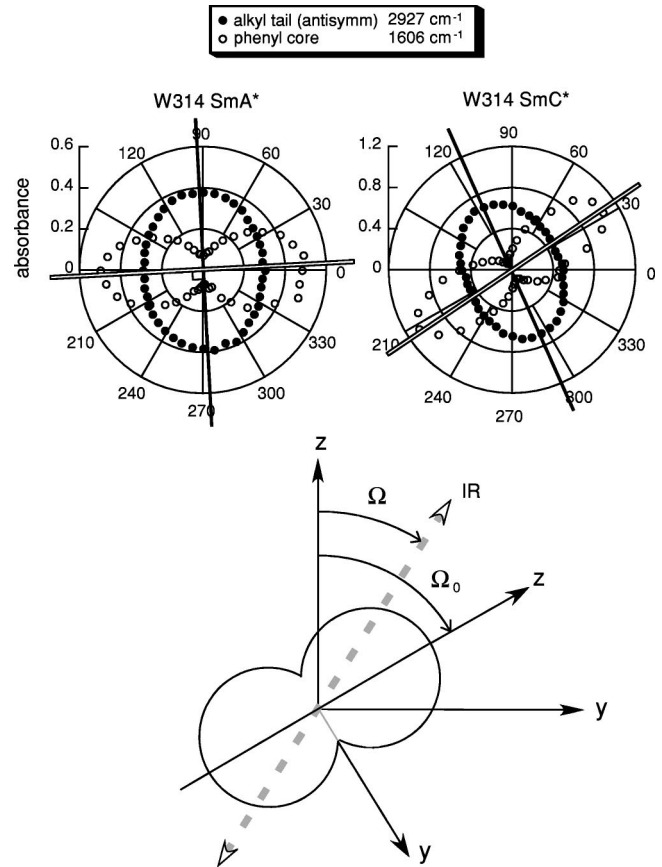
FIG. 3. Absorbance $A(\Omega)$ vs polarization orientation Ω for two representative stretching peaks (phenyl ring and antisymmetric alkyl CH$_2$ tail) of W314 at T=70 °C. In Sm-*C* phase, $\Delta\Omega_0(T) = \Omega_0(T)_{phenyl}-\Omega_0(T)_{alkyl}>0$ indicating a zigzag molecular shape.

(antisymmetric) stretching vibrational modes at 2927 cm^{-1} and for the C-C *phenyl* core stretching modes at 1606 cm^{-1}, respectively. This plot illustrates the dichroism and tilt angle from layer normal for each vibrational mode. Ignoring birefringence [28], $A(\Omega)$ for any mode must be of the form [13]

$$A(\Omega)=-\ln\{(10^{-A_{para}})\cos^2(\Omega-\Omega_0)$$
$$+(10^{-A_{perp}})\sin^2(\Omega-\Omega_0)\}, \qquad (1)$$

where the absorbances A_{para} (A_{perp}) are those measured with IR polarizer parallel (perpendicular) to the $\Omega=\Omega_0$ axis, an absorbance profile axis of mirror symmetry in Ω, where the polarizer orientation is for either maximum (A_{max}) or minimum (A_{min}) absorbance. Thus, Eq. (1) obtains for $A(\Omega)$ no matter what the molecular orientation distribution, with the three parameters A_{max}, A_{min}, and Ω_0 can be related to the three moments, $\langle p_y^2\rangle$, $\langle p_z^2\rangle$, $\langle p_y p_z\rangle$ of the mode absorption dipole **p**.

In the smectic-*A* phase, the absorbance of the phenyl (alkyl) vibration is maximum (minimum) for $\Omega\cong0$. Such differences may be quantitatively understood in terms of β, the angle between its absorption dipole and the mean molecular long axis; The *phenyl* core vibration has $\beta\sim0°$, and

thus, a large dichroism D ($\equiv A_{max}/A_{min}$) vs Ω, whereas the *alkyl* CH$_2$ stretching vibrations have $\beta \sim 90°$, for an all-trans tail, with the magnitude of the dichroism being reduced because of disorder in the tails. Since the transition dipole for the *phenyl* transition is generally parallel to the core [29], the coordinate system diagonalizing $\langle p_i p_j \rangle_{phenyl}$ has an axis parallel to the core, and $\theta_{phenyl} \equiv \Omega_0(T)_{phenyl}$ is a measure of the mean core orientation projected onto the tilt plane. By contrast, since the transition dipoles for the *alkyl* transitions are normal to an extended all-trans chain [parallel to the line in a CH$_2$ joining neighboring hydrogens vibrating out of phase (*anti*symmetric) and normal to the line for hydrogens vibrating in phase (*sym*metric)]. Thus, the coordinate system diagonalizing $\langle p_i p_j \rangle_{alkyl}$ has an axis parallel to an extended tail, and $\theta_{alkyl} \equiv \Omega_0(T)_{alkyl}$ is a measure of the mean tail orientation projected onto the tilt plane. What is typically found with respect to the phenyl and alkyl absorbance patterns is illustrated for Sm-*A* and Sm-*C* phases in W314 in Fig. 3. At T=100 °C in the Sm-*A* phase $\theta_{phenyl} \cong 0°$ and asymmetric $\theta_{alkyl} \cong 0°$, reflecting its uniaxial symmetry. At T=70 °C in the Sm-*C* phase, the tilt from **z** of the mirror reflection axis of $A(\Omega)$ closest to **z**, (maximum phenyl, minimum alkyl absorbance) is smaller for the asymmetric alkyl mode $[\theta(T)_{alkyl}=24°]$ than for the phenyl mode $[\theta(T)_{phenyl}=29°]$. The axis orientations of maximum phenyl and *maximum* alkyl absorbance orientations are drawn in Fig. 3 to indicate this difference in angle. The negative value of $\Delta \theta \equiv \theta_{alkyl} - \theta_{phenyl}$ suggests that the tails are less tilted than the cores. IR dichroism experiments have been carried out over wide temperature ranges in Sm-*C* phases of a variety of materials by us, and by Kim *et al.* [12] on the achiral tail of MHPOBC [32], to be discussed below. Zigzag behavior, with the tail absorbance tilted from **z** through a smaller angle than that of the phenyl is the norm, as illustrated in Figs. 4–6, although $\Delta \theta$ is typically smaller than that found in W314 and W399.

Additionally, the dichroic ratio of the alkyl band, $D_{alkyl,sym}=(A_{max}/A_{min})_{alkyl,sym}$ is much closer to one than that of the phenyl. Since $D=1$ indicates isotropic distribution of absorption dipoles in the tilt plane, the reduced dichroic ratio is indicative of orientational disorder in the chains. If we consider a binary model in which a chain is divided into two distinct regions, the region near the end is isotropically distributed and the region near the core perfectly ordered with the chain tilted through an angle θ relative to **z**, then the apparent tilt of the alkyl dichroism pattern will always be that of the tilted region, *even if it constitutes only a small fraction of the chain*, since adding in more isotropically distributed units cannot change the orientation of the absorbance pattern. Thus, as the ratio of the size of the isotropic to ordered regions increases, the tilt of the dichroism pattern will stay fixed, even though the average tilt of chain units is decreasing, indicating that the tilt of the alkyl dichroism pattern *does not directly* give information about the average tilt of the tail units. This will be discussed in greater detail in computer simulation below.

B. Optic axis orientation

The optical tilt angle, the orientation of the principal axis of the visible-light dielectric tensor, measured via polarized
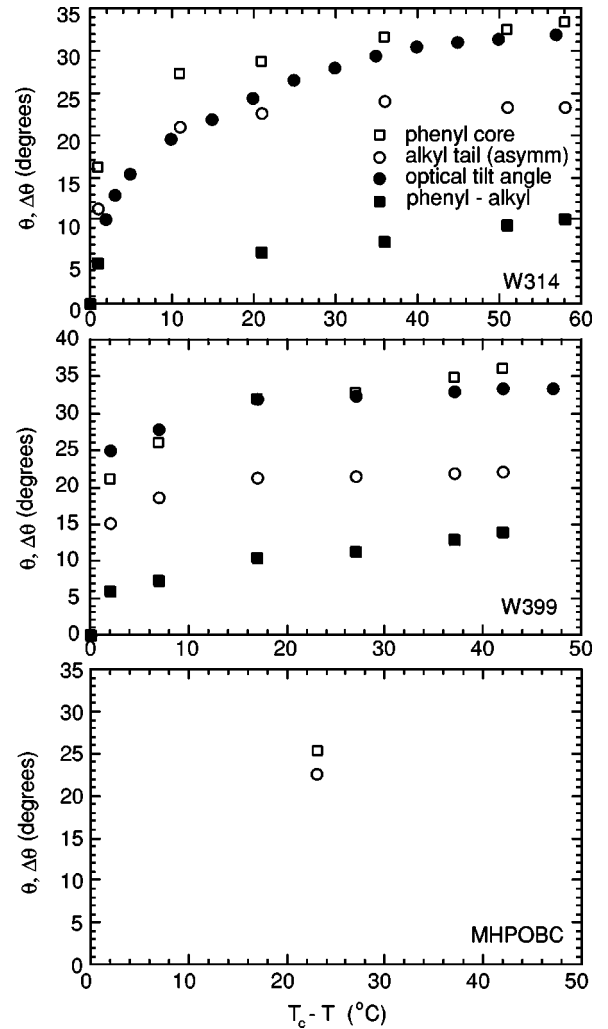
FIG. 4. Tilt angles from the layer normal of phenyl and alkyl profiles, $\theta(T)_{phenyl}$ and $\theta(T)_{alkyl}$, and zigzag angle $\Delta \theta(T) = \theta(T)_{phenyl} - \theta(T)_{alkyl}$ as a function of temperature in smectic-*C* phase in W314. Optic axis measurement from polarization microscopy is also displayed.

light microscopy, is shown in Fig. 4 for W314 and W399. The optical tilt is mainly determined by the core-tilt angle, because of the large optical anisotropy, of the core, a result of its rigidity and large longitudinal polarizability [30]. Since $\Omega_0(T)_{phenyl}$ is a good measure of the actual core tilt, it is comparable to the optic axis tilt, slightly larger possibly because of the contribution of the less tilted tails to the birefringence.

C. Layer spacing

1. X-ray data

The x-ray measurement of layer spacing provides information on molecular conformation in the Sm-*C* phase. We begin by assuming that the net change in layer spacing upon molecular tilt is simply due to the tilt of molecular segments, assuming that they are normal to the layers in the Sm-*A* phase. Then,
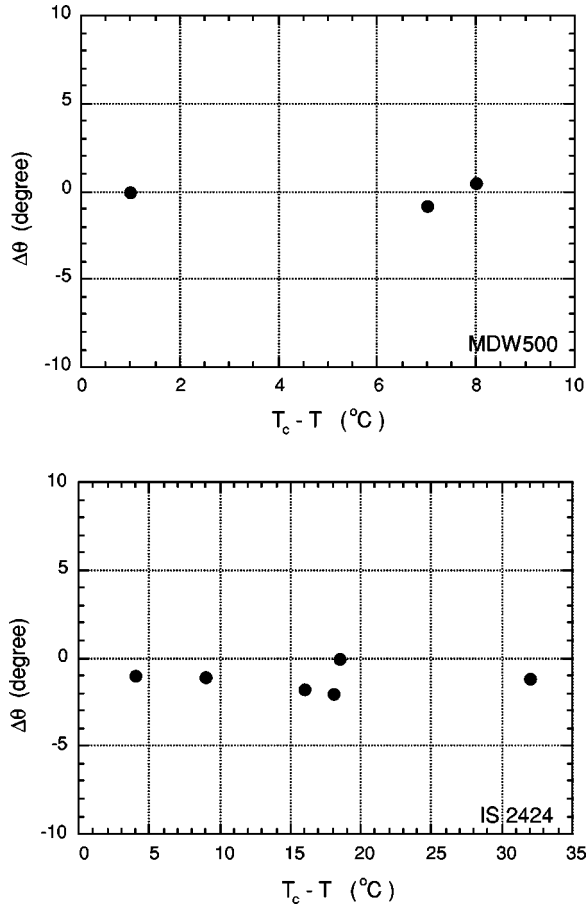
FIG. 5. Zigzag angles $\Delta\theta(T)=\theta(T)_{phenyl}-\theta(T)_{alkyl}$ for MDW500 and IS2424.

$$\frac{\delta l}{l}=\frac{\sum_i \langle l_i \cos \theta_i \rangle}{\sum_i l_i}, \qquad (2)$$

where $\delta l/l$ is the fractional change in layer thickness l as molecular segments of length l_i tilted by angle θ_i in the Sm-C phase, relative to that in the Sm-A phase. We further assume a division of molecules into tail (alkyl) and core (phenyl) segments, take as θ_i the IR determined θ_{alkyl} and θ_{phenyl}, and determine l_{alkyl} and l_{phenyl} from the all-trans molecular conformation. In this case, the $\delta l/l$ and its phenyl and alkyl contributions obtained for a variety of materials is shown in Fig. 7. The results show that this procedure leads to an excessively large overall shrinkage in all cases, especially in light of the remarkable fact for many materials $\delta l/l$ is nearly accounted for by core tilt alone. Since the core is rigid and the IR tilts match the observed visible-light optical tilts, it is difficult to see how the excessively large $\delta l/l$ could arise from misinterpretation of the core data. Thus, assignment of θ_{alkyl} to the whole length of the tail is the problem, the contribution of the alkyl tails to the layer shrinkage being much less than that obtained assuming a uniform θ_{alkyl}, implying that most of the tail segments are tilted by less, or are
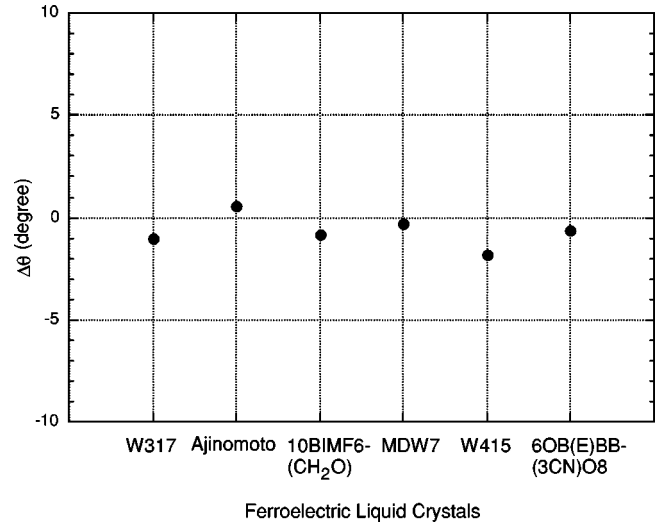
FIG. 6. $\Delta\theta=\theta_{alkyl}-\theta_{phenyl}$ of core-alkyl tail profiles for several FLC's. Most of the materials studied show small zigzag effects.

already tilted in the Sm-A phase and do not significantly tilt further in the Sm-C phase. We employ computer simulation to probe this issue further.

2. de Vries behavior

An essential complication in interpreting the change in the smectic layer spacing is that the molecules may be already tilted in the Sm-A phase. Indeed, the observation that the tail tilt does not significantly contribute to layer shrinkage implies that a significant fraction of tail segments are tilted in the Sm-A phase. In the extreme de Vries [31] limit, the molecules are fully tilted in the Sm-A and there is no layer shrinkage upon entering the Sm-C, simply an evolution from an isotropic distribution on the cone to a localized one.

Evidence for the de Vries Sm-A behavior from FTIR is provided by measuring the IR dichroism of the phenyl stretch mode. Tilt of molecules away from the layer normal in Sm-A necessarily reduces the phenyl dichroic ratio D_A. Such a reduction is evident in W314 and W399 in which D_A increases by nearly a factor of two from the Sm-A phase to the saturated Sm-C phase (from $D_A=5.82$ to 14.7 and 4.18 to 9.41, respectively). This strongly suggests de Vries-type behavior. Indeed, a simple model for the orientational distribution of the core indicates molecular tilt in the Sm-A phase of W314. The model assumes a Gaussian molecular tilt angle distribution $f(\theta)=C\exp\{-[(\theta-\theta_0)/2\sigma]^2\}$ centered at θ_0 with distribution width σ and isotropic azimuthal distribution. Figure 8 shows the possible range of $\theta_0(\sigma)$ and distribution width σ that gives rise to the observed Sm-A dichroism ($D_A=5.82$) of W314. There is significant tilt in all cases. The observed layer shrinkage of W314, $\delta l \cong l_{core}(\cos\theta_{core}-1)$, suggests that W314 is closer to $\theta_0=0$, since in the other limit one would expect $dl\sim0$.

D. Computer simulation

1. Large scale atomistic simulation

To characterize the molecular organization of the Sm-C phase in more detail and, in particular, to provide a detailed
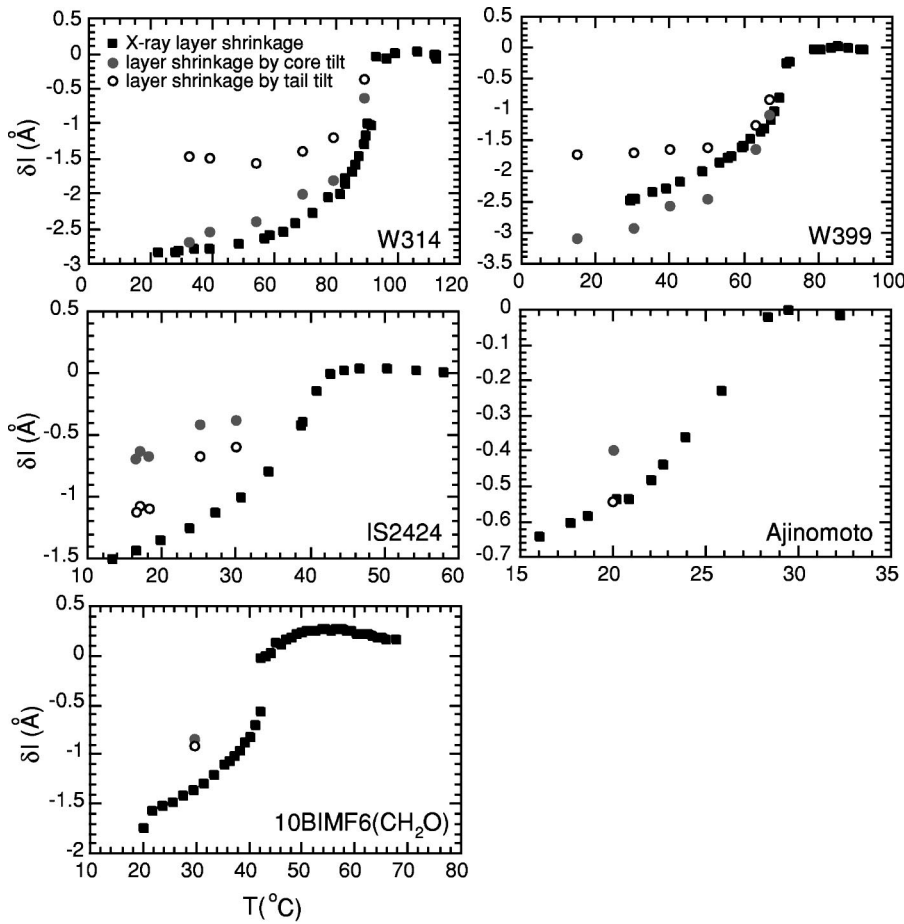
FIG. 7. The x-ray layer shrinkage of W314, W399, IS2424, Ajinomoto, and 10BIMF6(CH$_2$O) upon entering the Sm-C phase are shown. Core and tail tilt contributions to the layer shrinkage from IR data and Eq. (2) are also displayed for comparison, which shows that the assumption of rigid core and tail with IR tilts gives too much layer shrinkage, overestimating the tail contribution.

interpretation of the zigzag effect observed in polarized IR measurements, we have analyzed results from an extensive atomistic simulation study of MHPOBC. A more extensive discussion of this simulation will appear elsewhere [33].

The chemical structure and phase sequence of MHPOBC are shown in Fig. 2. In addition to Sm-A and Sm-C phases,

MHPOBC exhibits an antiferroelectric Sm-C_A phase and ferrielectric Sm-C_α and Sm-C_γ phases [20]. MHPOBC exhibits a zigzag effect similar to that observed in W314 and W399. Specifically, polarized IR spectroscopy measurements in the Sm-C phase show that the apparent tilt angle of the *achiral* tail of MHPOBC is smaller than that of the core, shown in
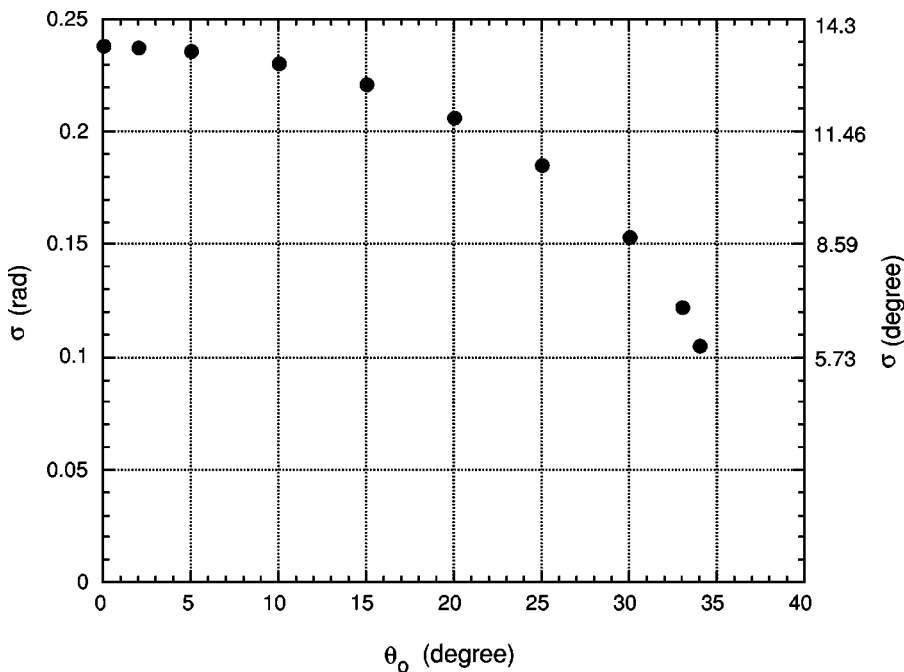
FIG. 8. Relations between $\theta_\bigcirc$ and width σ of Sm-A Gaussian molecular tilt angle distribution $f(\theta) = C \exp\{-[(\theta-\theta_0)/2\sigma]^2\}$ to give the observed phenyl dichroic ratio of W314 ($D_A = 5.82$).

Fig. 4 (the chiral tail of MHPOBC has a bent configuration putting it nearly parallel to the layers, leading to its antiferroelectric character) [32,33].

We carried out a 14.56 ns N-P-T (constant molecular numbers, pressure, and temperature) molecular-dynamics simulation of MHPOBC at $P=1$ atm and $T=363$ K, which is in the Sm-C_A phase range. Our simulations utilized a hybrid representation for hydrogen atoms, in which hydrogens bonded to sp^2-hybridized atoms (e.g., in phenyl rings) were represented as explicit interaction sites, while sp^3-hybridized CH_n groups were treated as spherically symmetric united atoms. We employed an interaction potential containing valence (bond stretch, bond angle bend, dihedral torsion, and inversion) interactions as well as nonbonded (van der Waals and Coulomb) site-site interactions. Most interaction parameters were derived from *ab initio* quantum chemical calculations at the $MP2/6\text{-}31G(d)//RHF/6\text{-}31G(d)$ level of theory, with the exception of van der Waals parameters, for which literature values optimized for liquid-state simulations were used [34,35]. The general procedure used to parametrize the interaction potential has been described previously [36], and a detailed description of the molecular model for MHPOBC will appear elsewhere [33].

Long-range Coulomb interactions were evaluated to high accuracy using the particle-mesh Ewald method [37], and a standard long-range correction for van der Waals interactions [38] was employed to account for pair interactions beyond the real-space interaction cutoff of 10 Å. The computational cost of the simulations was significantly reduced through use of a stable, highly optimized multiple-timestep molecular-dynamics integrator [39,40] with five distinct intervals for force evaluation, corresponding to bond stretching (0.417 fs), bond angle bending (0.833 fs), dihedral torsion (1.667 fs), short-range nonbonded (5 fs), and long-range electrostatic interactions (10 fs). The weak-coupling algorithm of Berendsen *et al.* [41] was used to maintain constant pressure and temperature.

The simulated system consisted of 100 molecules arranged in smectic layers in a monoclinic unit cell, with periodic boundary conditions. Although the long dimension of the unit-cell spans four smectic layers, there are only two distinct smectic layers in the system, owing to the rather unconventional unit-cell shape in which each smectic layer is connected to its next-nearest neighbor across the periodic boundary. This unit-cell geometry was chosen to promote homogeneity of ordering within each distinct smectic layer and to minimize finite-size artifacts related to the effective constraint of a constant number of molecules per smectic layer (the time scale for permeation of molecules between smectic layers is long compared with the time scale of the simulation). Notice also that this choice permits either synclinic (Sm-C) or anticlinic (Sm-C_A) ordering to develop without the creation of defects or domain walls.

A Sm-A-like initial condition was used, with molecules arranged in perfect smectic layers with their long axes oriented, with equal probability, either parallel or antiparallel to the layer normal, with random orientations about their long axes, and with random positions within the smectic layers. To promote anticlinic (Sm-C_A) ordering, a strong

(1000 V/μm) ''sublattice'' electric field was applied to the system during the first 5.06 ns of the simulation, with the field acting on molecules in the first smectic layer directed along $+y$, and that acting on molecules in the second layer directed along $-y$ (recall that there are only two distinct layers in the system). Here, the y axis is the axis normal to the plane of symmetry of the monoclinic unit cell. After removal of the sublattice electric field, the system was equilibrated for a further 4.5 ns, and thermodynamic averages were computed over the final 5 ns of the simulation.

The initial and final configurations from the simulation are shown in Fig. 9. Well-developed anticlinic ordering is apparent in the final configuration. In fact, spontaneous molecular tilt develops within the first ns of the simulation, and anticlinic ordering is already well established by the time the sublattice electric field is removed (after ~ 5 ns). In Fig. 10, we have displayed the final configuration, with molecular cores and chiral and achiral tails shown separately. Clearly, cores and tails are confined to well-defined sublayers, and the achiral tails appear to be tilted relative to the layer normal, although they exhibit considerable orientational and conformational disorder. The chiral tails display a high degree of conformational and orientational disorder, the origins of which will be discussed elsewhere [33]. The focus of the present discussion is on the behavior of the core and the *achiral* tail.

To compare the results of this simulation with experimental results on the Sm-C* phase of MHPOBC, we converted each anticlinic configuration from the simulation to a ''pseudo-synclinic'' configuration by rotating all molecules in one of the two smectic layers by π about the layer normal. The implicit assumption (which we feel is reasonable) is that the molecular-scale organization of the system (in particular, the zigzag ordering) is relatively insensitive to its clinicity. For example, x-ray scattering experiments on MHPOBC show that there is no measurable change in smectic layer spacing upon switching from the antiferroelectric state to a ferroelectric state under an applied electric field [42], which implies that the molecular organization of each smectic layer is essentially the same in both states.

The average smectic layer spacing from simulation is $d=31.0$ Å, nearly 10% smaller than the experimental layer spacing at 90 °C, $d=34.0$ Å. As discussed in more detail below, this implies that our model of MHPOBC underestimates the thickness of the alkyl tail sublayer. This in turn implies that our model overestimates (by $\sim 10\%$) either the average mass density of the tail sublayer or the in-layer area per molecule. Alkyl tails that are too highly tilted or conformationally disordered could lead to an in-layer area per molecule that is higher than experiment, for example. In fact, the simulated mass density of $\rho=1.046$ g/cm^3 is close to the experimental mass density of W314 at 90 °C, $\rho=1.021$ g/cm^3, which supports the conformationally disordered tail sublayers.

We estimated the thickness of the core and tail sublayers by measuring distributions of end-to-end distances l_{ee} for molecular cores and tails [$P(l_{ee})$], as well as distributions of lengths of end-to-end vectors projected onto the layer normal direction [$P(l_\parallel)$] shown in Fig. 11. In particular, we take the
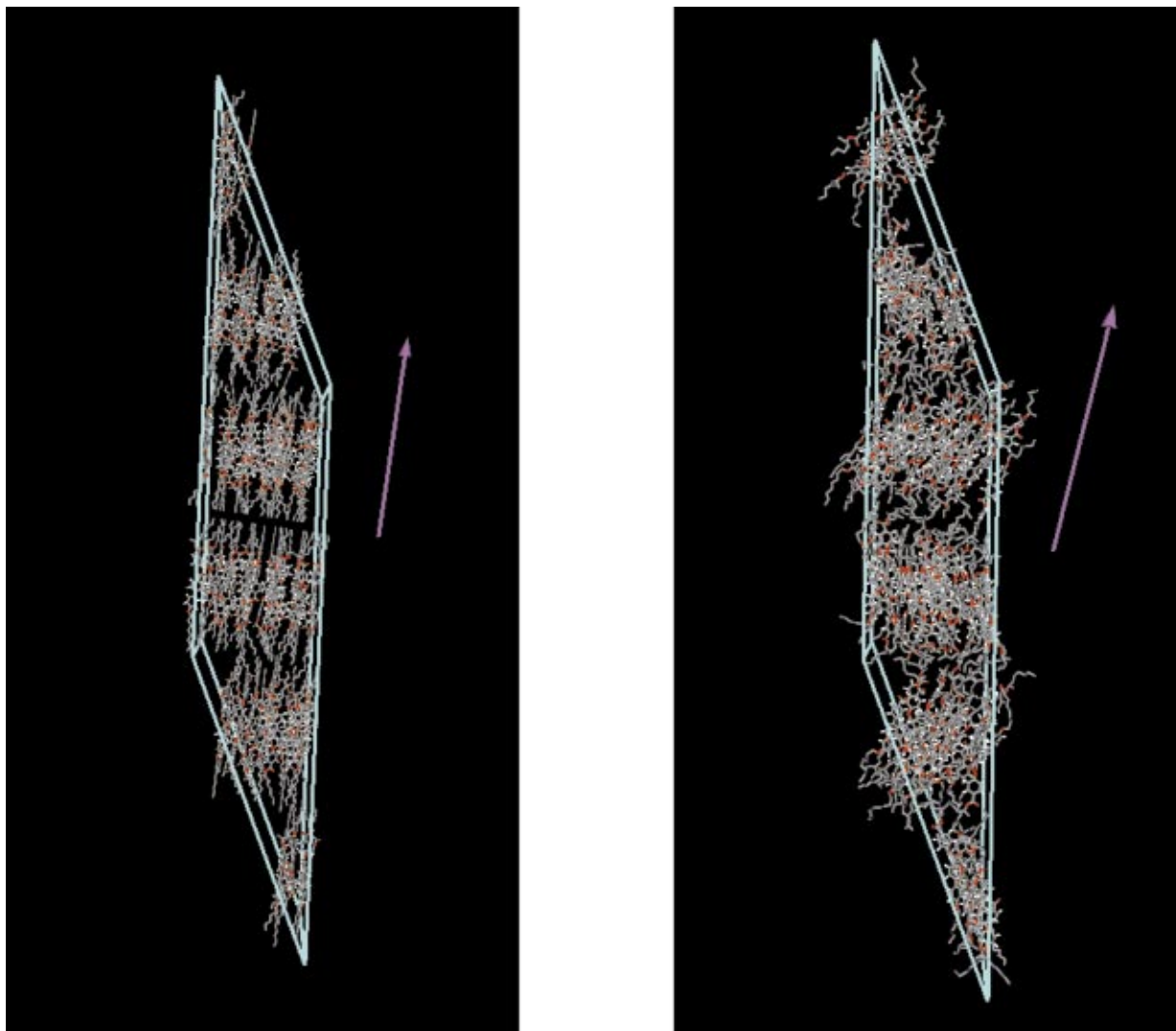
FIG. 9. (Color) The initial and final configurations from molecular-dynamics simulation of MHPOBC, showing well-developed anticlinic ordering in final configuration. The arrows indicate smectic layer normal.

most probable value of $l_\parallel$ for a given molecular substructure [corresponding to the position of the maximum in $P(l_\parallel)$] as our estimate of the sublayer thickness. The end-to-end distance for the core was measured from the ether oxygen atom in the achiral alkoxy tail to the carbonyl carbon in the chiral carboxylate tail, that of the achiral tail was measured from the ether oxygen to the terminal methyl carbon, and that of the chiral tail from the carbonyl carbon to the terminal methyl carbon.

Not surprisingly, $P(l_{ee})$ for the relatively rigid core is sharply peaked at 18.15 Å, which corresponds precisely to the fully extended length of the core determined from the AM1-optimized geometry. $P(l_\parallel)$ for the core is peaked at 16.85 Å, so our estimate of the thickness of the core sublayer is $d_{core} = 16.85$ Å. Note, also, that d_{core} is quite close to $l_{ee}^{max} \cos(\theta_{phenyl})$, as expected (for saturated molecular tilt, azimuthal fluctuations are small and do not cause the apparent and local tilt angles to be significantly different). l_{ee}^{max} for the achiral and chiral tails are measured to be 8.85, and 6.85 Å, respectively, somewhat smaller than the fully extended

lengths of 9.84 and 7.49 Å, respectively, reflecting some degree of conformational disorder in the alkyl chains. From $P(l_{ee})$, we find $d_{achiral} = 7.85$ Å, and $d_{chiral} = 5.45$ Å, which implies that the tails are tilted to some degree, and that the chiral tail is more highly tilted than the achiral tail on average. The total layer spacing should be approximately equal to the sum of the core and tail sublayer spacings, plus a quantity proportional to the van der Waals diameter of the terminal methyl group ($\sigma_{methyl} = 3.93$ Å). Here, we take the constant of proportionality to be $\sqrt{2/3}$, appropriate for a hexagonal close-packed arrangement of methyl groups at the layer interface, which gives $d \approx d_{core} + d_{achiral} + d_{chiral} + \sqrt{2/3}\sigma_{methyl} = 33.36$ Å. This is close to the average layer spacing of 31.0 Å, measured in the simulation, which suggests that our estimates of the core and tail sublayer spacings are reasonable.

2. Simulation calculation of IR dichroism

The IR dichroism and apparent tilt angle were calculated for three distinct absorption bands of the MHPOBC achiral
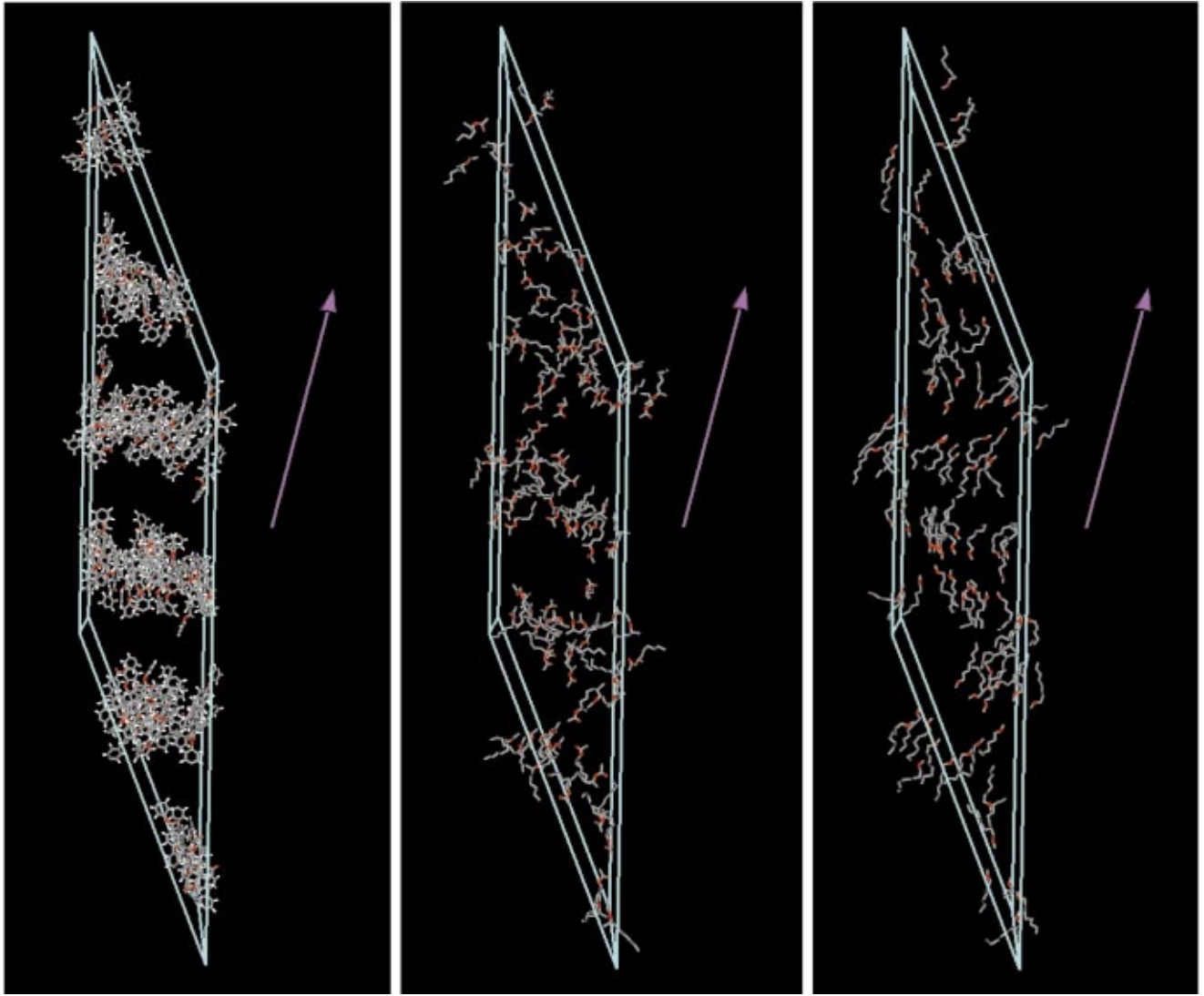
FIG. 10. (Color) Final configuration from molecular-dynamics simulation of MHPOBC, showing the molecular cores (left), chiral tails (center), and achiral tails (right). The arrows indicate smectic layer normal.

tail and core, associated with the methylene symmetric stretch mode (2856 cm^{-1}), the methylene asymmetric stretch mode (2927 cm^{-1}), and the phenyl longitudinal stretch mode (1606 cm^{-1}), for IR radiation propagating in the y direction (normal to the tilt plane). We assume that the IR absorption transition moment for the methylene symmetric stretch mode bisects the C-C-C or O-C-C bond angle centered on the methylene group, the methylene asymmetric stretch transition moment is normal to the plane of the C-C-C or O-C-C bond angle, and the phenyl stretch transition moment is along the *para* axis of the phenyl ring. The average absorbance is given by

$$A \propto C \langle (\hat{\mathbf{m}} \cdot \hat{\mathbf{E}})^2 \rangle = C \hat{\mathbf{E}} \cdot \langle \hat{\mathbf{m}} \hat{\mathbf{m}} \rangle \cdot \hat{\mathbf{E}}, \qquad (3)$$

where $\hat{\mathbf{m}}$ is the transition moment for a specific mode, $\hat{\mathbf{E}}$ is the electric-field direction, and summation over repeated indices is implied in Eq. (3) [43]. The dichroic ratio is the ratio of the maximum and minimum eigenvalues of the 2×2 or-

dering tensor $\langle \hat{\mathbf{m}} \hat{\mathbf{m}} \rangle$, and the apparent tilt angle is the orientation of the principal eigenvector of $\langle \hat{\mathbf{m}} \hat{\mathbf{m}} \rangle$ relative to its orientation in the Sm-A phase.

IR absorbances often represent averages over several distinct functional groups, which complicates the interpretation of apparent tilt angle measurements. In particular, the apparent tilt for methylene symmetric and antisymmetric stretch modes represents an average over all methylene groups in a molecule, while the apparent tilt determined from phenyl stretch modes represents an average over all phenyl groups. In this average, functional groups possessing a higher degree of orientational anisotropy contribute relatively more to the overall dichroism and, therefore, to the apparent tilt angle. For example, if all methylene groups except one are isotropically distributed, then the apparent tilt angle measured via polarized IR spectroscopy is simply the tilt angle of the single anisotropic methylene. Although this is an extreme example, evidence from computer simulation (presented below) suggests that this is a better description of typical ma-
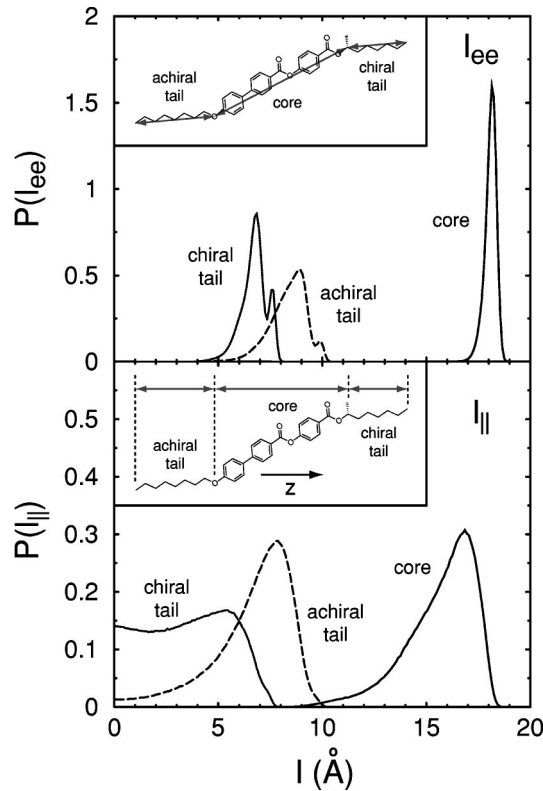
FIG. 11. (a) Distributions of end-to-end distance l_{ee} for molecular cores and tails $P(l_{ee})$ in the MHPOBC. (b) Distributions of lengths of end-to-end vectors projected onto the layer normal direction $P(l_\parallel)$.

FIG. 12. (a) Labeling of CH_2 groups in the achiral tail of MHPOBC referred to in the text and in TableI. (b) Labeling of interatomic vectors in the achiral tail of MHPOBC referred to in the text and in Table II.

terials than an extended all-trans chain, i.e., that methylene groups closest to the LC core exhibiting greater orientational anisotropy and therefore contributing more heavily to the apparent tilt angle than methylene groups more distant from the core (a consequence of the conformational flexibility of the alkyl tails).

These arguments are reasonably well supported by Fig. 12, and Tables I and II for the computer simulation of achiral tail of MHPOBC. Table I shows dichroic ratios D_{seg} and tilt angle θ_{seg} for the symmetric and antisymmetric stretch modes of individual methylene segments in the achiral tail of

MHPOBC from computer simulation. Table II shows tilt angle and nematic order parameters of interatomic vectors in the achiral tail of MHPOBC, obtained from simulation. Table III shows dichroic ratios D and tilt angle θ obtained from simulation with average over all methylene segments indicated by Greek letters as shown in Fig. 12. Methylene segment α has considerably higher dichroic ratios both in symmetric and antisymmetric stretching modes than any other methylene segments, indicating that methylene groups closer to core indeed possess higher-order orientational anisotropy (dichroism values decrease as distance from the core increases). Moreover, mean tilt angles θ_{seg} for α symmetric and asymmetric stretching modes are also significantly larger ($25.2°$ and $23.3°$) than other methylene subgroups, and very close to experimental value ($24°$). Therefore, although we add more methylene subgroups β, γ, ..., the overall tilt angle increases very little, being determined by that of methylene subgroup α. Figure 12 and Table II show tilt angles and nematic order parameters of interatomic vectors in the achiral tail of MHPOBC obtained from simulation. Vectors that are closer to core exhibit larger tilt angles with significantly higher-order parameters S, again supporting our argument. The simulations reproduce well the systematic trends of the tilt dichroism data.

TABLE I. Mean dichroic ratios D_{seg} and tilt angles θ_{seg} for the symmetric and antisymmetric stretch modes of individual methylene segments shown in Fig. 12 in the achiral tail of MHPOBC, obtained from simulation.

	D_{seg}		θ_{seg} (degree)	
Methylene	Sym	Antisym	Sym	Antisym
α	3.10	4.33	25.2	23.3
β	1.65	3.63	11.3	21.4
γ	1.63	2.06	12.9	18.1
δ	1.78	2.38	12.6	18.3
ϵ	1.64	1.83	13.2	15.1
ζ	1.49	1.88	11.8	16.2
η	1.34	1.41	12.2	12.0

TABLE II. Tilt angles and nematic order parameters of interatomic vectors shown in Fig. 12 in the achiral tail of MHPOBC, obtained from simulation.

Vector	θ_S (degree)	S
1	25.8	0.55
2	24.4	0.63
3	18.4	0.46
4	16.2	0.35
5	16.2	0.41
6	14.9	0.33
7	15.1	0.31
8	13.0	0.20

TABLE III. Comparison of dichroic ratios D and apparent tilt angles θ obtained from simulation with experimental values for selected vibrational modes of the core and achiral tail of MHPOBC. The tail tilt angles θ_{alkyl} are obtained by averaging over the θ_{seg} values of Table I.

| | D | | θ (degree) | |
Mode	Simulation	Experiment [a]	Simulation	Experiment [a]
Alkyl sym	1.70	2.12	15.7	17.2
Alkyl antisym	2.22	1.83	19.0	20.0
Phenyl	18.7	22.3	24.4	23.9

[a]Reference [32].

about each molecular conformation and orientation in tilted smectics. The materials W314, W399, and MHPOBC turned out to possess the most distinctive ''zigzag'' molecular structures with tails clearly less tilted from layer normal than cores. Comparison of x-ray-measured layer shrinkage with that calculated from the IR-measured core and tail tilt data shows that in these materials, layer shrinkage in Sm-*C* arises almost entirely from the core tilt, and that for all materials studied, the tails shrink less upon tilting than calculated from their IR measured tilt. Atomistic computer simulation of MHPOBC enabled us to show that this difference is due to the disordering of the tails, with only the part near the core contributing to the layer shrinkage and dominating the IR tilt.

IV. CONCLUSION

We have carried out polarized IR absorption spectroscopy and x-ray diffraction that provides us with useful information

ACKNOWLEDGMENTS

[1] R.B. Meyer, L. Liebert, L. Strzelecki, and P. Keller, J. Phys. (France) **36**, L-69 (1975).

[2] N.A. Clark and S.T. Lagerwall, Appl. Phys. Lett. **36**, 899 (1980).

[3] R. Bartolino, J. Doucet, and G. Durand, Ann. Phys. (Leipzig) **3**, 389 (1978).

[4] E.N. Keller, E. Nachaliel, D. Davidov, and C. Böffel, Phys. Rev. A **34**, 4363 (1986).

[5] D.M. Walba and N.A. Clark, Proc. SPIE **825**, 81 (1987).

[6] M.D. Wand, R. Vohra, D.M. Walba, N.A. Clark, and R. Shao, Mol. Cryst. Liq. Cryst. **202**, 183 (1991).

[7] D.M. Walba, Ferroelectrics **1**, 5090 (1991).

[8] D.M. Walba and N.A. Clark, Ferroelectrics **84**, 65 (1988).

[9] D.J. Photinos and E.T. Samulski, Science **270**, 783 (1995).

[10] M.A. Glaser, V.V. Ginzburg, N.A. Clark, E. Garcia, D.M. Walba, and R. Malzbender, Mol. Phys. Rep. **10**, 26 (1995).

[11] M.A. Glaser and N.A. Clark, Liq. Cryst. (to be published).

[12] K.H. Kim, K. Ishikawa, H. Takezoe, and A. Fukuda, Phys. Rev. E **51**, 2166 (1995).

[13] W.G. Jang, C.S. Park, J.E. Maclennan, K.H. Kim, and N.A. Clark, Ferroelectrics **180**, 213 (1996).

[14] F. Hide, N.A. Clark, K. Nito, A. Yasuda, and D.M. Walba, Phys. Rev. Lett. **75**, 2344 (1995).

[15] A. Kocot, J.K. Vij, and T.S. Perova, Adv. Chem. Phys. **113**, 203 (2000).

[16] D.M. Walba, M.B. Ros, N.A. Clark, R. Shao, M.G. Robinson, J.Y. Liu, K.M. Johnson, and D. Doroski, J. Am. Chem. Soc. **113**, 5471 (1991).

[17] W.G. Jang, C.S. Park, and N.A. Clark, Phys. Rev. E **62**, 5154 (2000).

[18] K.E. Arnett, D.M. Walba, and J.A. Drewes, in Thin Films for Integrated Optics Applications, edited by B.W. Wessels and D.M. Walba, MRS Symposia Proceedings No. 392 (Materials Research Society, Pittsburgh, 1995); p. 135; D.M. Walba, D.J. Dyer, P.L. Cobben, T. Sierra, J.A. Rego, C.A. Liberko, R. Shao, and N.A. Clark, in Thin Films for Integrated Optics Applications, edited by B.W. Wessels and D.M. Walba, MRS Symposia Proceedings No. 392 (Materials Research Society, Pittsburgh, 1995), p. 157.

[19] P.A. Williams, L. Komitov, A.G. Rappaport, B.N. Thomas, N.A. Clark, D.M. Walba, and G.W. Gray, Liq. Cryst. **14**, 1095 (1993).

[20] A.D.L. Chandani, Y. Ouchi, H. Takezoe, A. Fukuda, K. Terashima, K. Furukawa, and A. Kishi, Jpn. J. Appl. Phys., Part 2 **28**, L1261 (1989).

[21] R. Eidenschink, T. Geelhaar, G. Andersson, A. Dahlgren, K. Flatischler, F. Gouda, S.T. Lagerwall, and K. Skarp, Ferroelectrics **84**, 167 (1988).

[22] G. Scherowsky, B. Brauer, K. Grüneberg, U. Müller, L. Komitov, S.T. Lagerwall, K. Skarp, and B. Stebler, Mol. Cryst. Liq. Cryst. **215**, 257 (1992).

[23] Displaytech, Inc.

[24] D.M. Walba (unpublished).

[25] Ajinomoto Chemical, Inc.

[26] Kashima Petroleum, Inc. Japan.

[27] Chisso Chemical, Japan.

[28] Equation (1) is exact only in absence of birefringence (optical anisotropy in the real part of the dielectric constant), when the eigenmodes of a dichroic medium are linearly polarized along the directions of maximum and minimum absorbance. For the vibrations studied here, polarized nearly along the optic axis of the real part of the dielectric constant, the birefringence can be ignored in few micron thick samples.

[29] The transition dipole for the *phenyl* transition is generally parallel to the core.

[30] J.W. Goodby, R. Blinc, N.A. Clark, S.T. Lagerwall, M.A. Osipov, S.A. Pikin, T. Sakurai, K. Yoshino, and B. Žekš, *Ferroelectric Liquid Crystals* (Gordon and Breach, New York, 1991).

[31] A.J. de Vries, Mol. Cryst. Liq. Cryst. **41**, 27 (1977).

[32] B. Jin, Z. Ling, Y. Takanishi, K. Ishikawa, H. Takezoe, A. Fukuda, M. Kakimoto, and T. Kitazume, Phys. Rev. E **53**, R4295 (1996).

[33] M.A. Glaser, Y. Lansac, M. Nendel, W.G. Jang, and N.A. Clark (unpublished).

[34] W.L. Jorgensen, J.D. Madura, and C.J. Swenson, J. Am. Chem. Soc. **106**, 6638 (1984); J.M. Briggs, T. Matsui, and W.L. Jorgensen, J. Comput. Chem. **11**, 958 (1990); W.L. Jorgensen, E.R. Laird, T.B. Nguyen, and J. Tirado-Rives, *ibid.* **14**, 206 (1993); J.M. Briggs, T.B. Nguyen, and W.L. Jorgensen, J. Phys. Chem. **95**, 3315 (1991).

[35] J.I. Siepmann, S. Karaborni, and B. Smit, Nature (London) **365**, 330 (1993).

[36] M.A. Glaser, N.A. Clark, E. Garcia, and D.M. Walba, Spectrochim. Acta, Part A **53**, 1325 (1997).

[37] U. Essmann, L. Perera, M.L. Berkowitz, T. Darden, H. Lee, and L.G. Pedersen, J. Chem. Phys. **103**, 8577 (1995).

[38] M.P. Allen and D.J. Tildesley, *Computer Simulation of Liquids* (Clarendon Press, Oxford, 1987).

[39] M. Tuckermann, B.J. Berne, and G.J. Martyna, J. Chem. Phys. **97**, 1990 (1992).

[40] J.C. Sexton and D.H. Weingarten, Nucl. Phys. B **380**, 665 (1992).

[41] H.J.C. Berendsen, J.P.M. Postma, W.F. van Gunsteren, A. Dinola, and J.R. Haak, J. Chem. Phys. **81**, 3684 (1984).

[42] Y. Takanishi, A. Ikeda, H. Takezoe, and A. Fukuda, Phys. Rev. E **51**, R400 (1995).

[43] J. Michl and E.W. Thulstrup, *Spectroscopy with Polarized Light* (VCH, New York, 1986).